

Time- and Strain-Dependent Nanoscale Structural Degradation in Phase Change Epitaxial Strontium Ferrite Films

Le Wang,^{1†} Zhenzhong Yang,^{1†} Jinpeng Wu,² Mark E. Bowden,³ Wanli Yang,² Amy Qiao,⁴ Yingge Du^{1*}

¹Physical and Computational Sciences Directorate, Pacific Northwest National Laboratory, Richland, Washington 99354, United States.

²Advanced Light Source, Lawrence Berkeley National Laboratory, Berkeley, California 94720, United States.

³Environmental Molecular Sciences Laboratory, Pacific Northwest National Laboratory, Richland, Washington 99354, United States.

⁴Energy and Environment Directorate, Pacific Northwest National Laboratory, Richland, Washington 99354, United States.

[†]These authors contributed equally to this work.

*Corresponding author. E-mail: Yingge.du@pnl.gov

Abstract

Topotactic phase transition between metallic, perovskite SrFeO₃ and insulating, Brownmillerite SrFeO_{2.5} has been extensively studied due to the potential applications in resistive switching devices for neuromorphic computing. However, its practical utilization as memristors has been hindered by the structural instability of SrFeO₃, which is often ascribed to the generation of oxygen vacancies to form SrFeO_{3-δ}. Here we reveal the dominating defects generated in SrFeO₃ epitaxial thin films are atomic scale gaps as a result of interfacial strain. Our correlated time- and strain-dependent measurements show that tensile strained SrFeO₃ films form vertical, nanoscale gaps that are SrO-rich, which are accountable for the observed metal-to-insulator transition over time. While compressively strained or small lattice mismatched SrFeO₃ films mainly yield horizontal gaps with a smaller impact on the in-plane transport. The atomic scale origin of such defects and their impact on device performance need to be further understood in order to integrate phase change materials in oxide electronics.

Introduction

Perovskite-structured strontium ferrite SrFeO_3 , together with its sub stoichiometric oxides $\text{SrFeO}_{3-\delta}$ (SFO), have attracted great attention due to their rich structural, physical, and chemical properties.¹⁻¹⁰ In particular, as illustrated in Fig. 1a, the reversible topotactic phase transition occurring between SrFeO_3 and the reduced Brownmillerite-structured $\text{SrFeO}_{2.5}$ has been shown to induce resistive switching phenomena,^{9, 11-13} which have been investigated as memristors for their potential use in neuromorphic computing devices.⁷ While epitaxial growth of such materials in thin film form offers a scalable way to integrate them in oxide electronics, there are still several challenges hindering their practical applications. For example, bulk SrFeO_3 can be readily synthesized through high-pressure and high-temperature techniques, but SFO thin films grown by molecular beam epitaxy (MBE) or pulsed laser deposition (PLD) have been shown to contain significant amount of oxygen vacancies (V_{O}) due to the low oxygen partial pressure employed.^{7, 12, 14, 15} Recently, it has been shown that the use of more oxidizing agent (e.g., oxygen plasma or ozone) during the synthesis and subsequent processing can lead to fully oxidized SrFeO_3 .¹⁵⁻¹⁷ However, the long-term stability of stoichiometric, metallic SrFeO_3 films were found to be not reliable, which has been tentatively ascribed to the instability of Fe^{4+} .¹⁶⁻¹⁸ The exact mechanism remains unclear due to the lack of time-dependent structural and chemical characterization at the atomic scale. Given that the realization of resistive-switching-based oxide electronics depend critically on the materials' stability, the origin for such structural evolution and conductivity decay needs to be further understood.

In this study, we investigate the time- and strain-dependent atomic and electronic structural evolutions in a set of well-defined SFO films with discrete strain conditions. We show that as a result of interfacial strain, atomic-scale defect planes to nanoscale defect gaps can develop in stoichiometric SrFeO_3 films after the oxidation process. While majority of the films remain metallic SrFeO_3 , the highly localized defect gaps are found to be SrO-rich, and thus can dominate the transport behavior. While a tensile strain generally favors the generation of gaps vertical to the substrate, a compressive strain or small lattice mismatch can yield defect gaps parallel to the substrate. As a result, films under tensile strain display much quicker conductivity decay compared to compressively strained SFO films. The physical origins of such nanoscale

defects and their impact on device integration need to be further studied in order to use strontium ferrite and similar phase change materials in future oxide electronics.

Results

Brownmillerite-Perovskite Phase transition

Differently strained perovskite SrFeO₃ films used in this study were obtained by annealing of PLD-grown SrFeO_{2.5} films in oxygen plasma (see Experimental section). Figure 1b shows representative X-ray diffraction (XRD) θ - 2θ patterns of the as-grown (BM SrFeO_{2.5}), air-annealed (SrFeO_{3- δ}), and plasma-annealed (SrFeO₃) thin films on (001)-oriented SrTiO₃ (STO) substrates with a 25 nm thickness, respectively. The distinct thickness fringes around Bragg peaks (Fig. 1c) suggest good crystalline quality for all three cases. In addition to the (001) diffraction peaks, the observed half-order peak in SrFeO_{2.5} indicates that the ordered oxygen vacancy channels are parallel to the thin film surface,^{19,20} which is determined by our growth parameters and consistent with previous reports.^{6,11,15} On the other hand, the air annealed and plasma-annealed samples show complete suppression of the half-order peaks from the BM phase and the SFO film diffraction peaks shift to higher angles, indicating the reduction in out-of-plane (c-axis) lattice parameters. The decrease in the c-axis lattice parameter from 4.008 Å to 3.855 Å for the air-annealed sample indicates that significant amount of oxygen vacancies in the BM-SFO's tetrahedral sub-lattices are healed. However, the air annealed SFO film still shows a semiconductor behavior (Fig. 1e), suggesting that it is not fully stoichiometric. In contrast, the SFO film resulting from plasma annealing shows a further reduction in c-axis lattice parameter (3.832 Å) and metallic conductivity (Fig. 1e). The resistivity of the plasma annealed perovskite SrFeO₃ film at room temperature is about 1 mΩ.cm, consistent with previous reports.^{1,16,21} The measured c-axis lattice parameter is smaller than that of bulk SrFeO₃ (3.850 Å),¹ as a result of the in-plane tensile strain applied by the STO. X-ray direct space mappings (DSM) near the (103) reflection of STO (Fig. 1d) reveal that all three films are coherently strained to the STO substrates without lattice relaxation.

Conductivity decay over time

For the plasma annealed SFO film grown on STO shown in Fig. 1e, we tracked its long-term in-plane transport properties as a function of time. Figure 2a shows the evolution of resistivity versus temperature relationships. A three-fold decrease in room-temperature conductivity is observed just one day after plasma annealing. In addition, the in-plane transport behavior of the film became semiconducting and the overall resistivity increases continuously with time. Hong *et al.*¹⁶ reported that the increase in resistivity of the SFO thin film was related to the c-axis expansion and argued that it was presumably due to the creation of oxygen vacancies. Acting as electron donors, oxygen vacancies could reduce Fe⁴⁺ to Fe³⁺ and increase the ionic radius of the Fe ion. The more Fe³⁺ in SFO, the higher the resistance and the bandgap.^{3, 6, 15} In order to evaluate whether oxygen vacancy formation plays a role in the observed resistivity change, we also performed time-dependent XRD and spectroscopic ellipsometry (SE) measurements. Figure 2b shows the XRD patterns around the (002) diffraction peak over time. It is clear that albeit the continuous change in resistivity, the change in SFO (002) diffraction peaks is almost negligible with a tiny shift to the smaller angle (the c-axis lattice parameter changing from 3.832 Å (initial) to 3.834 Å (32 days)). DSM scans with time (Fig. S1) show that the SFO film is still fully strained to the STO substrate after exposure in air for 32 days. As the c-axis lattice parameter of SFO is very sensitive to the oxygen vacancies (see discussion in Fig. 1), the small change (<0.1%) in c-axis lattice parameter indicates that SFO retains the perovskite phase, where Fe in SFO is mostly in the nominal state of Fe⁴⁺ after exposure in air for 32 days. Moreover, the optical absorption spectra derived from SE (Fig. 2c) show no obvious difference over time. According to the previous reports,^{17, 22} the absorption feature *B* is associated with the split-off empty Fe 3d e_g/O 2p hybridized band resulting from Fe⁴⁺. As shown in Fig. 2c, the feature *B* does not show obvious change with time, suggesting that the Fe valence is mostly Fe⁴⁺, consistent with XRD results. The onset of optical transition *B* determined by Tauc plots (Fig. S2) still shows 0 eV after exposed the sample in air for more than one month, indicating the film should retain its metallic behavior. Combined measurements based on ensemble-averaged techniques all suggest that there is little to no detectable changes in materials' structure, therefore oxygen vacancies should not be the main cause for the observed changes in resistivity.

Strain effect

Note that this unstable metallic phase of perovskite SrFeO₃ is not limited to the films grown on STO substrates, as conductivity decays with different magnitudes have also been observed in plasma annealed SFO films on various substrates with different strain states (see Fig. 3). In bulk, SrFeO₃ is a cubic structure with a lattice constant of 3.850 Å. Hence, SrFeO₃ experiences compressive strain of -1.58% on LaAlO₃ (LAO), and tensile strains of +0.46%, +1.41%, and +2.53% on (LaAlO₃)_{0.3}(Sr₂AlTaO₆)_{0.7} (LSAT), STO and DyScO₃ (DSO) (Fig. 3a), respectively. As shown in Fig. 3b, after plasma annealing (initial), SFO films on LAO, LSAT or STO display comparable metallic behaviors, in good agreement with the 0 eV bandgap derived from the SE data (Fig. S3). However, the initial state of the plasma annealed SFO film on DSO is too resistive to measure based on our current experimental setup, although it also shows a perovskite phase (Fig. S4) with near zero bandgap (Fig. S3). After exposed in air for 5 days, SFO on LSAT still shows the metallic behavior with a slight increase in resistivity across temperature range. On the other hand, SFO films on LAO and STO show the insulator behavior with one and four orders of magnitude changes in resistivity, respectively. Figure 3c plots time-dependent resistivity changes measured at room temperature for films grown on these four substrates. It is clear that SFO on lattice matched LSAT undergoes the least change. For all other three cases (except SFO on DSO, which is too resistive to measure), the rate of conductivity decay is found to be faster during the first several days until a seemingly plateau is reached. For the compressively strained SFO on LAO, the resistivity increased over an order of magnitude, while the tensile strained SFO on STO showed an increase over four orders of magnitude. Such a strong strain dependence may indicate atomic scale defects, such as misfit dislocations, which are known to impact the in-plane transport properties.^{23, 24} To determine the atomistic mechanism for the structural and electronic structure evolutions of SrFeO₃ on different substrates, we performed high-resolution scanning transmission electron microscopy (STEM) analysis for these plasma annealed SFO films within a few days after plasma annealing. Figure 3d-3g show the cross-sectional high-angle annular-dark-field STEM (HAADF-STEM) images for different samples taken along [100] direction. The prevalent, alternating contrast with double periodicity of the perovskite structure shown in the films is due to the formation of Brownmillerite structures, which could be induced by using focused ion beam during the TEM sample preparation process. The electron beam during STEM imaging may also induce perovskite-Brownmillerite phase transition.¹⁵ Compared to the as-

grown BM-SFO, the striking difference displayed by plasma-annealed samples here is the much higher contrast lines, either parallel (LAO and LSAT) or perpendicular (STO and DSO) to the substrates. These lines correspond to defect planes (gaps) along the beam projection direction. For SFO on DSO, the defect gaps are ~ 2 nm in width which allowed the surface Au coatings deposited during TEM sample preparation to permeate. Such large-scale defect gaps can greatly impact the in-plane transport and explain why SFO on DSO was too resistive to measure. Comparing the other three STEM images with the time-dependent resistivity evolution shown in Fig. 3c, we can further analyze how the atomic-scale gaps impact conductivity.

In order to probe the structural and chemical change in the gap region, we performed high-resolution electron energy loss spectroscopy (EELS) analysis on the SFO/LAO sample (as shown in Fig. 4a). The elemental mappings reveal that the gap regions are Fe and O deficient with local Sr rich. Sr segregation in perovskite oxides is a known problem to deteriorate oxygen reduction kinetics and suppress the oxygen evolution reaction (OER),²⁵⁻²⁷ and Sr leaching has been observed after the acidic OER process.^{26, 28} In principle, Sr segregation layer is more likely to be in the form of SrO.²⁹ Because SrO is a wide bandgap insulator, the existence of the vertical SrO rich gaps can be considered as local resistors in serial connection in an in-plane transport setup, as illustrated in Fig. 4d, contributing the overall semiconducting behavior albeit the SFO islands are metallic. With humidity exposure, SrO is easy soluble in the water and thus strongly impact the in-plane transport properties (see the model plotted in Fig. 4d). The defect gaps formed in SFO on STO ($\epsilon=+1.41\%$) are vertical to the substrate and can be explained why the conductivity of SFO/STO decays faster. As for SFO on LSAT ($\epsilon=+0.46\%$), the dominating defect gaps are oriented parallel to the substrate, which may adversely affect the vertical transport properties, but has less impact on the in-plane transport, which can explain why the conductivity of this sample decays the slowest. For SFO on LAO ($\epsilon=-1.58\%$), in addition to horizontal gaps, there are some vertical gaps near the surface region. However, the vertical gaps do not penetrate throughout the film, which leaves pathways for electrical conduction, rendering a slower decay compared to SFO/STO. We further investigated water-induced changes in structural stability and transport properties of a plasma-annealed SFO/LAO. DI water soaking (see the inset of Fig. 4b) should lead to large change in resistivity as the excess SrO is water soluble. Indeed, we show that a quick, 5 sec DI water exposure leads to two orders of magnitude increase in the resistivity (Fig.

4b), with an accompanied metal-to-insulator transition without color change (see the inset of Fig. 4b). Four orders of magnitude change is observed when the water soaking time is increased to 60 sec. Significant structural changes are also observed at the vicinity of the gap regions after soaking as shown in the STEM image (Fig. 4c).

In addition, we also checked X-ray absorption spectroscopy (XAS) across Fe *L* edge (Fig. 3h) and O *K* edge (Fig. 3i) for the following samples: as grown BM SrFeO_{2.5} on STO (SrFeO_{2.5}), plasma annealed SFO on LSAT with 2 days exposed in air (LSAT 2 days), and plasma annealed SFO on STO with 10 days and 25 days exposed in air (STO 10 days and STO 25 days). The Fe *L*₃ spectrum of SrFeO_{2.5} exhibits a strong peak at ~702.8 eV (indicated by the dashed line) with another pronounced peak at ~701.6 eV (marked by the arrow), consistent with Fe³⁺ observed in other rare-earth ferrites, such as LaFeO₃ and EuFeO₃.^{30,31} After plasma treatment, the intensity of the peak at around 701.6 eV decreases and there is a clear, ~0.2 eV shift of the major peak to higher photon energy, indicating that plasma treatment leads the transition from Fe³⁺ to Fe⁴⁺.³ In addition, the FWHM of Fe *L*-edge XAS spectra becomes larger for the plasma treated samples. O *K* edge absorption spectra (Fig. 3i) further confirms the transition from Fe³⁺ to Fe⁴⁺ through the pre-edge Fe-O hybridization features. For SrFeO_{2.5}, the pre-edge structure from 528 to 533 eV is very similar to that of the brownmillerite SrFeO_{2.46} reported by Galakhov *et al.*³ A strong pre-peak feature is observed for the other three measurements with plasma treatment (marked by blue arrow), which is attributed to the Fe³⁺→Fe⁴⁺ transition.^{3,7,9,17,30} While the spectra difference between LSAT 2 days and STO 10 days are subtle, the difference between STO 10 days and STO 25 days are more evident. As shown in Fig. 3h, the Fe *L* spectra becomes slightly narrower after aging for 25 days, indicating a partial reduction from Fe⁴⁺ to Fe³⁺, presumably occurring at the vicinity of gap regions close to the surface. The reduction in the intensity of the O *K*-edge pre-peak also corroborate with this assignment, suggesting that oxygen vacancies are created but are localized to the gap regions, which are insensitive to XRD and optical ellipsometry. Therefore, we can conclude that the vertical gaps formation and evolution during and after plasma treatment, and their further interaction with the environment should be the main driving force leading to the decay of metallicity in SFO.

Discussion

The facts that the initial state being metallic right after plasma annealing and no obvious difference in the conductivity of SFO films with various strain states (see Fig. 3b) indicate that the defect gaps or planes should develop after oxygen plasma treatment. Without more oxidizing agent (oxygen plasma), oxygen vacancies may develop due to the small formation energy barrier in SrFeO₃ (32), which can release the strain effect from substrates, leading to the formation of atomic-scale gaps. Tensile strain could easily form the defects along the vertical direction, and the formed atomic-scale defects (Sr segregation) will quickly propagate from the surface to the interface region over time, resulting in vertical gaps we observed in Fig. 3. By contrast, compressive strain would form the horizontal defect planes.

Based on the above discussion, we can understand that the vertical gaps with SrO-rich in tensile strained SFO lead to a faster conductivity decay and metal-to-insulator transition. However, the retaining of good conductivity in SFO/LSAT may not indicate they are better suited for resistive switching applications, which require vertical integration. As shown in Fig. 3d and 3e, the horizontal defect gaps may severely impact the electron transport and oxygen diffusion along the film growth direction, which is required to promote the BM-P phase transitions during resistive switching. On the other hand, the existence of SrO-rich vertical gaps may not interfere with the nanoscale resistive switching phenomena, as the gap-separated SFO islands remain coherent to the substrates (Fig. S1). Our further experiments will address how the resistive switching properties are impacted by different types of such defect gaps by investigating SFO films grown on differently strained substrate, but with an SrRuO₃ thin film as a conductive buffer layer to form the heterojunction devices. Moreover, freestanding SFO films can release the strain effect,³³⁻³⁵ which may prevent these defect gaps formation after plasma treatment. This idea should be more intensively investigated in the future.

To summarize, our time- and strain-dependent studies involving XRD, SE, XPS, STEM and XAS demonstrate that perovskite SrFeO₃ films can undergo significant changes in their structural and electronic properties. However, the dominating defect is highly localized, nanoscale gaps instead of oxygen vacancies resulting from a topotactic phase transition. The SrO-rich defect gaps lead to the observed metal-to-insulator transition and an increase in resistivity. Our study highlights that long-term structural stability of phase change materials need to be addressed in order to harness their novel structural and electronic properties.

Experimental Methods

Thin films growth: High-quality epitaxial $\text{SrFeO}_{3-\delta}$ ($0 < \delta \leq 0.5$) thin films were grown on a set of single-crystalline substrates, including LAO, LSAT, STO and DSO, by using pulsed laser deposition.¹⁵ Samples were grown at 700 °C in oxygen partial pressure of 0.1 mTorr. After growth, the samples were cooled down to room temperature at the same oxygen partial pressure.

Oxidation treatment: In order to obtain fully oxidized SrFeO_3 films, the as-grown $\text{SrFeO}_{3-\delta}$ films were treated by air anneal and oxygen plasma anneal, respectively. For air anneal, the samples were transferred into a tube furnace and heated to 650 °C in ambient air for 5 hours and then cooled down to room temperature with 10 °C/min. For oxygen plasma anneal, the samples were transferred into a UHV chamber and heated to 600 °C in oxygen plasma at a chamber pressure of $\sim 3 \times 10^{-5}$ Torr for one hour and then cooled down to room temperature slowly. The specific oxygen plasma annealing treatment steps have been described in Ref. 17.

Structural characterization: XRD measurements were performed using a Rigaku SmartLab instrument with Cu $K\alpha 1$ radiation ($\lambda = 1.5406 \text{ \AA}$). The high-angle annular-dark-field (HAADF) micrographs of the films were obtained using an ARM200F (JEOL, Tokyo, Japan) STEM operated at 200 kV with a CEOS Cs corrector (CEOS GmbH, Heidelberg, Germany) to cope with the probe-forming objective spherical aberration. HAADF images were acquired at acceptance semi-angles of 90-370 mrad with a probe current of ~ 20 pA. The attainable resolution in HAADF images is better than 0.078 nm.

Electronic, optical and electrical characterization: XAS were carried out at Advanced Light Source (ALS) Beamline 8.0.1, located at Lawrence Berkeley National Lab (LBNL). All the spectra were normalized to the beam flux measured by the upstream gold mesh. The resolution of the excitation energy is 0.15 eV without considering core-hole lifetime broadening. Detailed procedures have been introduced in Ref. 36. Spectroscopic ellipsometry measurements and electrical resistivity measurements of SFO films have been described in Ref. 17.

Acknowledgments

The work is supported by an LDRD project within Chemical Dynamics Initiative at the Pacific Northwest National Laboratory (PNNL). PNNL is a multi-program national laboratory operated for DOE by Battelle. Initial sample growth was supported by U.S. Department of Energy (DOE), Office of Science, Office of Basic Energy Sciences, Early Career Research Program under Award No. 68278. J.W. would like to thank the financial support of the ALS postdoctoral fellowship. We acknowledge facility support from W. R. Wiley Environmental Molecular Sciences Laboratory, a DOE User Facility sponsored by the Office of Biological and Environmental Research. Soft X-ray spectroscopy data was performed at ALS of LBNL, which is supported by the Director, Office of Science, Office of Basic Energy Sciences, of the U.S. Department of Energy under Contract No. DE-AC02-05CH11231. We thank Drs. Scott A. Chambers, Tiffany Kaspar, Endong Jia, and Jinhui Tao for valuable discussions.

Author contributions: L. W., Z. Y. and Y. Du conceived this project. L. W. performed the epitaxial thin film synthesis, plasma processing, and ellipsometry spectroscopy measurements. L. W. and A. Q. performed in-plane electrical transport measurements and data analysis. M. E. B. performed XRD measurements and analysis. Z. Y. performed STEM/EELS measurements and data analysis. J. W. and W. Y. collected and analyzed the XAS data. L. W., Z. Y. and Y. D. co-wrote the manuscript. All authors discussed the results and commented on the manuscript.

Competing interests: The authors declare that they have no competing interests.

Additional information

Supporting Information is available online or from the author.

References

1. MacChesney, J., Sherwood, R., Potter, J., Electric and magnetic properties of the strontium ferrates. *J. Chem. Phys.* **43**, 1907-1913 (1965).
2. Takeda, T., Yamaguchi, Y., Watanabe, H., Magnetic structure of SrFeO₃. *J. Phys. Soc. Jpn.* **33**, 967-969 (1972).
3. Galakhov, V. et al., Valence band structure and X-ray spectra of oxygen-deficient ferrites SrFeO_x. *J. Phys. Chem. C* **114**, 5154-5159 (2010).
4. Yagi, S. et al., Covalency-reinforced oxygen evolution reaction catalyst. *Nat. Commun.* **6**, 8249 (2015).
5. Hirai K., et al., Melting of Oxygen Vacancy Order at Oxide–Heterostructure Interface. *ACS Appl. Mater. Interfaces* **9**, 30143-30148 (2017).
6. Khare, A. et al., Topotactic Metal–Insulator Transition in Epitaxial SrFeO_x Thin Films. *Adv. Mater.* **29**, 1606566 (2017).
7. Ge, C. et al., A Ferrite Synaptic Transistor with Topotactic Transformation. *Adv. Mater.* **31**, 1900379 (2019).

8. Kang, K. T. et al., A Room-Temperature Ferroelectric Ferromagnet in a 1D Tetrahedral Chain Network. *Adv. Mater.* **31**, 1808104 (2019).
9. Nallagatla, V. R. et al., Topotactic Phase Transition Driving Memristive Behavior. *Adv. Mater.* **31**, 1903391 (2019).
10. Nemudry, A., Weiss, M., Gainutdinov, I., Boldyrev, V., Schöllhorn, R., Room temperature electrochemical redox reactions of the defect perovskite $\text{SrFeO}_{2.5+x}$. *Chem. Mater.* **10**, 2403-2411 (1998).
11. Acharya, S. K. et al., Epitaxial brownmillerite oxide thin films for reliable switching memory. *ACS Appl. Mater. Interfaces* **8**, 7902-7911 (2016).
12. Saleem, M. S. et al., Electric field control of phase transition and tunable resistive switching in $\text{SrFeO}_{2.5}$. *ACS Appl. Mater. Interfaces* **11**, 6581-6588 (2019).
13. Tian, J. et al., Nanoscale Topotactic Phase Transformation in SrFeO_x Epitaxial Thin Films for High-Density Resistive Switching Memory. *Adv. Mater.* **31**, 1903679 (2019).
14. Khare, A. et al., Directing Oxygen Vacancy Channels in $\text{SrFeO}_{2.5}$ Epitaxial Thin Films. *ACS Appl. Mater. Interfaces* **10**, 4831-4837 (2018).
15. Wang, L., Yang, Z., Bowden, M. E., Du, Y., Brownmillerite phase formation and evolution in epitaxial strontium ferrite heterostructures. *Appl. Phys. Lett.* **114**, 231602 (2019).
16. Hong, D., Liu, C., Pearson, J., Bhattacharya, A., Epitaxial growth of high quality SrFeO_3 films on (001) oriented $(\text{LaAlO}_3)_{0.3}(\text{Sr}_2\text{TaAlO}_6)_{0.7}$. *Appl. Phys. Lett.* **111**, 232408 (2017).
17. Wang, L. et al., Hole-induced electronic and optical transitions in $\text{La}_{1-x}\text{Sr}_x\text{FeO}_3$ epitaxial thin films. *Phys. Rev. Mater.* **3**, 025401 (2019).
18. Enriquez, E. et al., Oxygen vacancy-driven evolution of structural and electrical properties in $\text{SrFeO}_{3-\delta}$ thin films and a method of stabilization. *Appl. Phys. Lett.* **109**, 141906 (2016).
19. Inoue, S. et al., Anisotropic oxygen diffusion at low temperature in perovskite-structure iron oxides. *Nat. Chem.* **2**, 213 (2010).
20. Jeon, H. et al., Topotactic phase transformation of the brownmillerite $\text{SrCoO}_{2.5}$ to the perovskite $\text{SrCoO}_{3-\delta}$. *Adv. Mater.* **25**, 3651-3656 (2013).
21. Yamada, H., Kawasaki, M., Tokura, Y., Epitaxial growth and valence control of strained perovskite SrFeO_3 films. *Appl. Phys. Lett.* **80**, 622-624 (2002).
22. Smolin, S. Y. et al., Static and Dynamic Optical Properties of $\text{La}_{1-x}\text{Sr}_x\text{FeO}_{3-\delta}$: The Effects of A-Site and Oxygen Stoichiometry. *Chem. Mater.* **28**, 97-105 (2015).
23. Du, Y. et al., Layer-resolved band bending at the n-SrTiO₃ (001)/p-Ge (001) interface. *Phys. Rev. Mater.* **2**, 094602 (2018).
24. Yun, H. et al., Uncovering the Microstructure of BaSnCb Thin Films Deposited on Different Substrates Using TEM. *Microsc. Microanal.* **24**, 2198-2199 (2018).
25. Chen, Y. et al., Impact of Sr segregation on the electronic structure and oxygen reduction activity of $\text{SrTi}_{1-x}\text{Fe}_x\text{O}_3$ surfaces. *Energy Environ. Sci.* **5**, 7979-7988 (2012).
26. Seitz, L. C. et al., A highly active and stable $\text{IrO}_x/\text{SrIrO}_3$ catalyst for the oxygen evolution reaction. *Science* **353**, 1011-1014 (2016).

27. Tsvetkov, N., Lu, Q., Sun, L., Crumlin, E. J., Yildiz, B., Improved chemical and electrochemical stability of perovskite oxides with less reducible cations at the surface. *Nat. Mater.* **15**, 1010 (2016).
28. Han, B. et al., Iron-based perovskites for catalyzing oxygen evolution reaction. *The J. Phys. Chem. C* **122**, 8445-8454 (2018).
29. Koo, B. et al., Sr segregation in perovskite oxides: why it happens and how it exists. *Joule* **2**, 1476-1499 (2018).
30. Abbate, M. et al., Controlled-valence properties of $\text{La}_{1-x}\text{Sr}_x\text{FeO}_3$ and $\text{La}_{1-x}\text{Sr}_x\text{MnO}_3$ studied by soft-x-ray absorption spectroscopy. *Phys. Rev. B* **46**, 4511 (1992).
31. Choquette, A. K. et al., Synthesis, structure, and spectroscopy of epitaxial EuFeO_3 thin films. *Cryst. Growth Des.* **15**, 1105-1111 (2015).
32. Das, T., Nicholas, J. D., Qi, Y., Long-range charge transfer and oxygen vacancy interactions in strontium ferrite. *J. Mater. Chem. A* **5**, 4493-4506 (2017).
33. Lu, D. et al., Synthesis of freestanding single-crystal perovskite films and heterostructures by etching of sacrificial water-soluble layers. *Nat. Mater.* **15**, 1255 (2016).
34. Hong, S. S. et al., Two-dimensional limit of crystalline order in perovskite membrane films. *Sci. Adv.* **3**, eaao5173 (2017).
35. Ji, D. et al., Freestanding crystalline oxide perovskites down to the monolayer limit. *Nature* **570**, 87 (2019).
36. Wu, J. et al., Elemental-sensitive detection of the chemistry in batteries through soft x-ray absorption spectroscopy and resonant inelastic x-ray scattering. *J. Vis. Exp.* **134**, e57415 (2018).

Figures

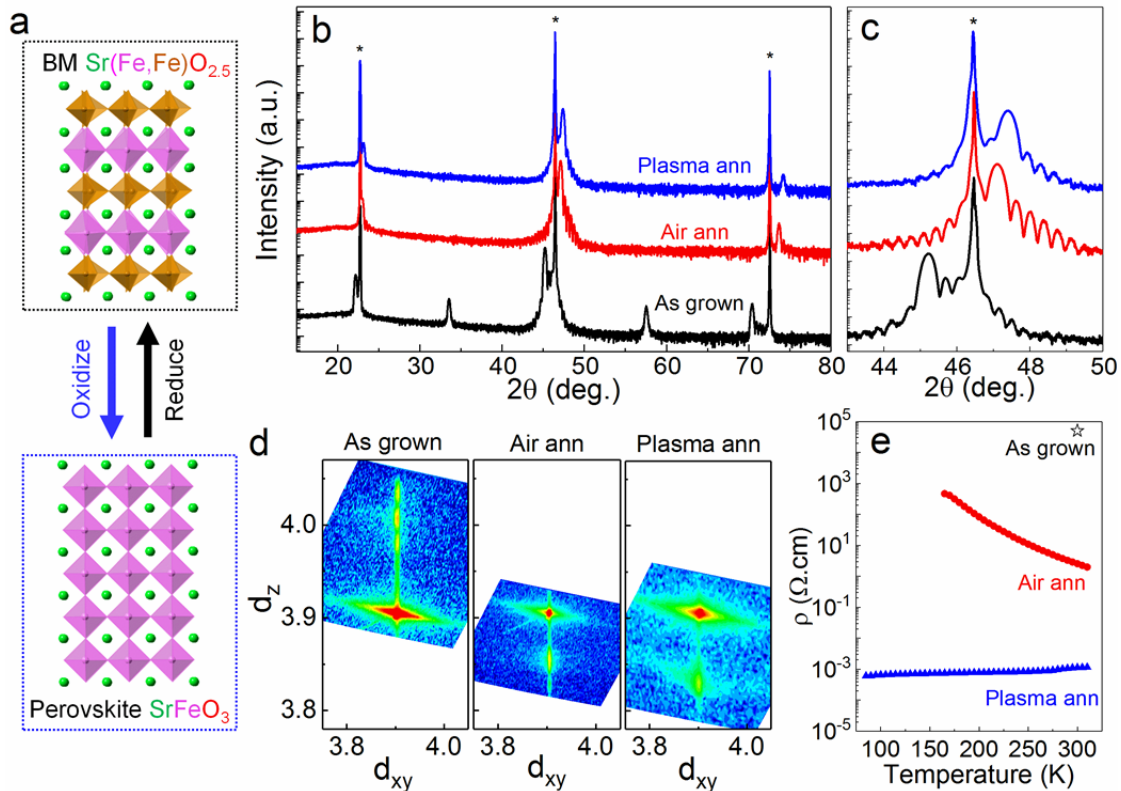


Fig. 1. Topotactic phase transition from brownmillerite (BM) SrFeO_{2.5} to perovskite (P) SrFeO₃. (a) Schematic diagrams of the reversible structure change between BM SrFeO_{2.5} and perovskite SrFeO₃ through oxidation and reduction. The crystal structures were viewed along the [100] direction. (b, c) X-ray diffraction (XRD) θ - 2θ scans of epitaxial SrFeO_{3- δ} (SFO) thin films on STO substrates. Stars indicate the diffraction peaks from STO substrates. As grown, air anneal (ann) and plasma ann denote three different states of SFO films. (d) DSMs of SFO thin films with three different states around the (103) Bragg reflection of the STO substrates, indicating SFO thin films without any lattice relaxation. (e) Resistivity (ρ) vs. temperature on heating for SFO thin films with three different states.

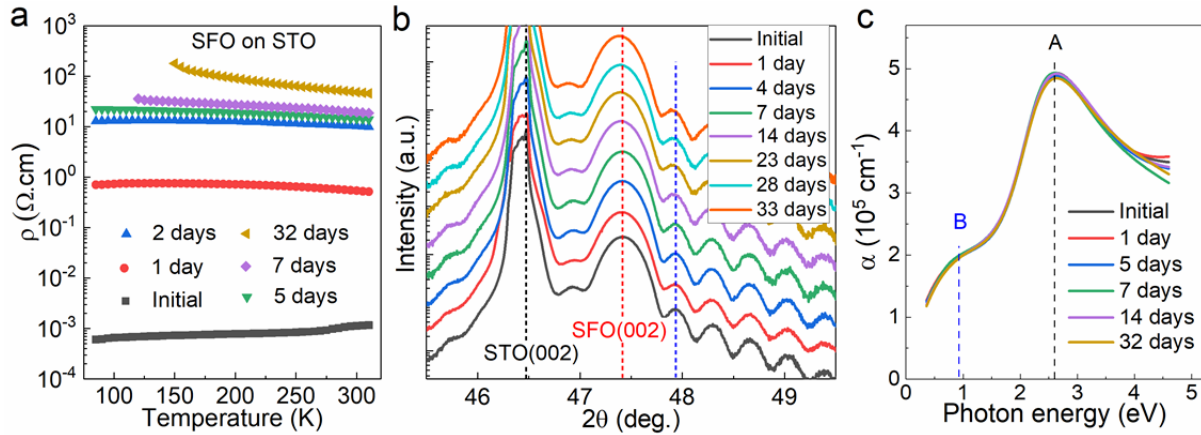


Fig. 2. Time dependent in-plane transport, structure and absorption measurements of plasma annealed SFO films. (a) ρ vs. temperature on heating, (b) XRD curves around the (002) diffraction peak, and (c) Absorption spectra measured after plasma annealing (initial), 1 day and several days exposed in air. The black and red dashed lines in (b) indicate the peak positions of the STO substrate and the initial state of plasma annealed SFO film, respectively. The blue dashed line in (b) denotes one thickness fringe. Characteristic features in the low-energy portion of the absorption spectra in (c) are defined as *a* and *b*.

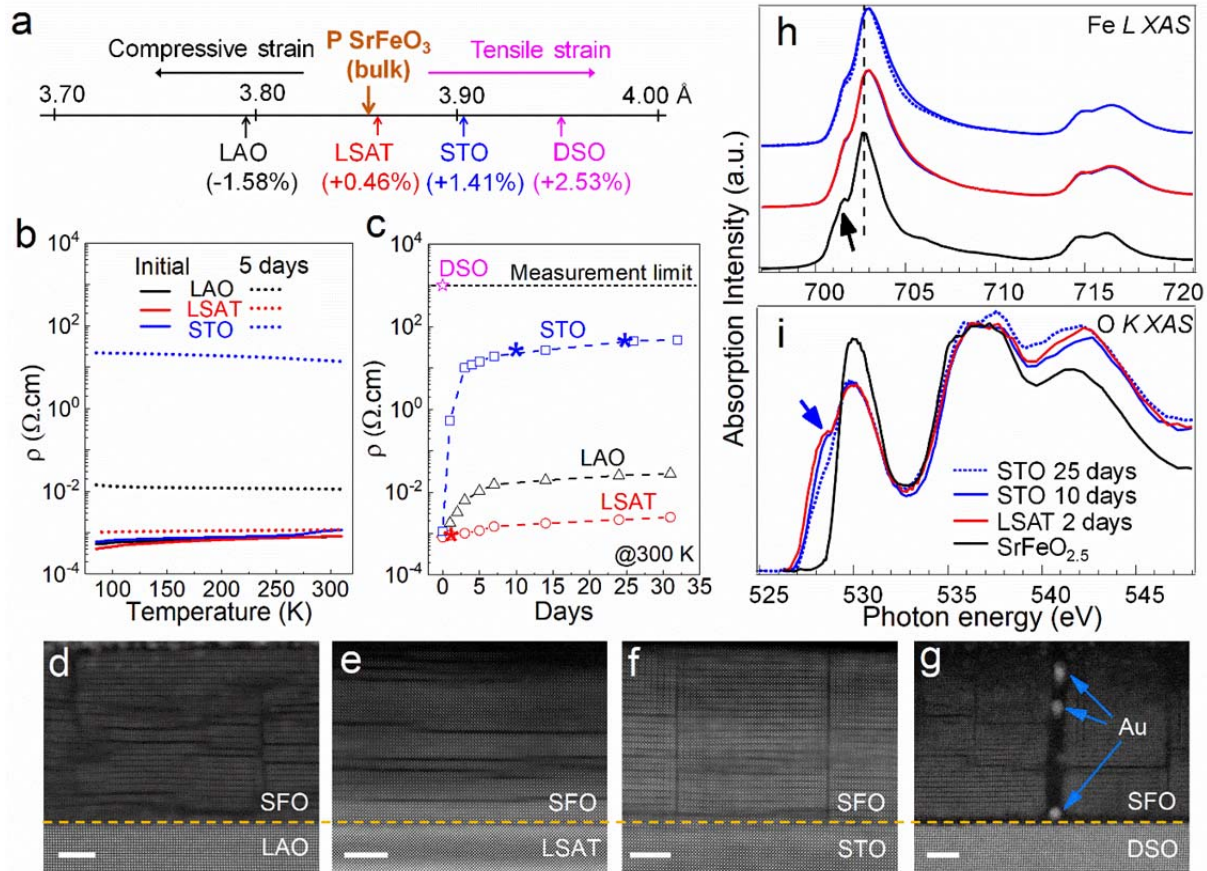


Fig. 3. Strain effect on the unstable metallic phase in perovskite (P) SrFeO₃ and the defect gap formation. (a) Lattice mismatch (ϵ) between the bulk P SrFeO₃ and the substrates used in this study. Pseudo-cubic lattice constants were used for noncubic substrates. (b) ρ vs. temperature curves for SFO films grown on different substrates measured after plasma anneal (initial) and 5 days exposure in air. (c) Room temperature ρ vs. time exposed in air for plasma annealed SFO films grown on different substrates. The stars represent the samples which an X-ray absorption spectrum (XAS) was acquired. (d-g) Cross-sectional HAADF-STEM images of the plasma annealed SFO films grown on (d) LAO, (e) LSAT, (f) STO and (g) DSO. The scale bar is 5 nm. The arrows in (g) denote the Au particles which diffused into the vertical gaps during Au top electrodes' deposition by sputtering. (h, i) XAS measured by total electron yield (TEY) detection mode across Fe *L* edge (h) and O *K* edge (i). Black, red and blue (dashed blue) denote the BM SrFeO_{2.5} on STO, the P SrFeO₃ on LSAT with 2 days exposed in air, and the P SrFeO₃ on STO with 10 (25) days exposed in air, respectively.

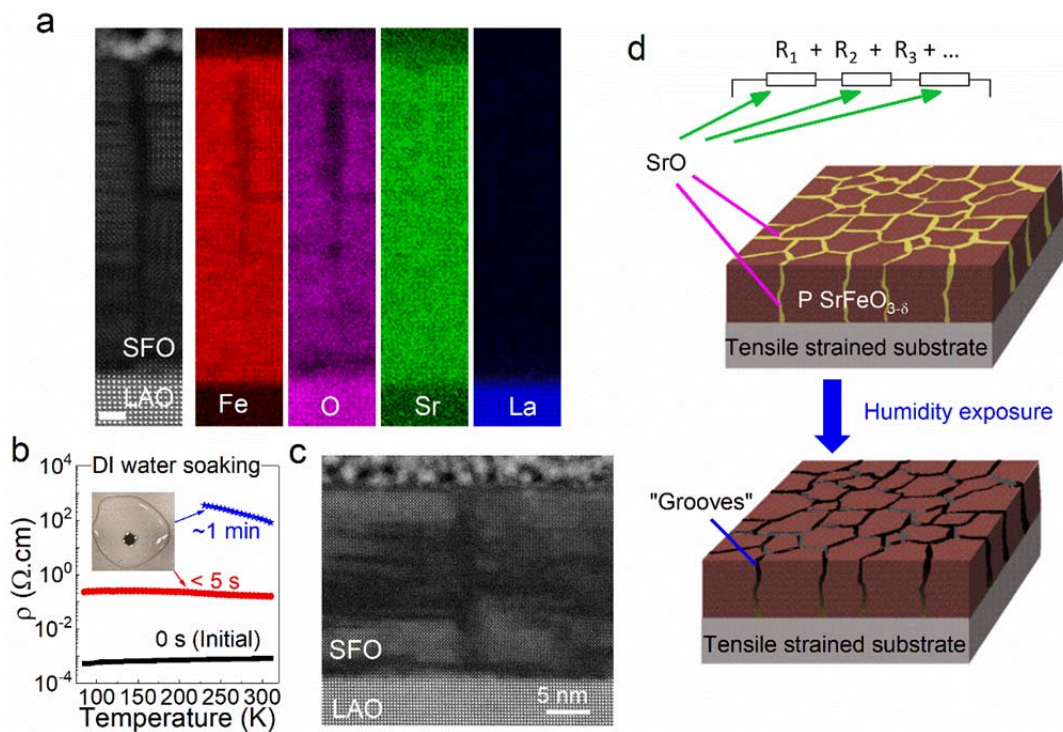


Fig. 4. Atomic scale understanding the unstable metallic phase in perovskite SrFeO_3 . (a) EELS maps for the vertical gap area of one plasma annealed SFO on LAO. The scale bar is 2 nm. (b) Resistivity change with DI water soaking. The inset shows the water soaking setup. (c) Cross-sectional HAADF-STEM image captured after DI water soaking. (d) Schematic of the main cause for the conductivity decay.